Conjunctive and complementary CA1 hippocampal cell populations relate sensory events to immobility and locomotion

Samsoon Inayat[1,3], Brendan B. McAllister[1], Bruce L. McNaughton[1,2], Ian Q. Whishaw[1], and Majid H. Mohajerani[1,3]

1. Canadian Centre for Behavioural Neuroscience, University of Lethbridge, Lethbridge, Alberta, Canada
2. Center for the Neurobiology of Learning and Memory, University of California, Irvine, California, USA
3. Corresponding authors: samsoon.inayat@gmail.com, mohajerani@uleth.ca

Abstract

The way in which the brain decodes signals from sensory activity related to ongoing behavior has revolutionized the understanding of the function of neocortical areas and provides a blueprint to address allocortical regions such as the hippocampus. Here two-photon calcium imaging of somal activity in hippocampal CA1 neuron populations was done in head fixed mice given air or light stimulation when at rest or when moving on a conveyor belt. Air stimulation was also used to induce running for a fixed distance on the conveyor belt by releasing a conveyor belt brake. Overall, 99% of 2083 cells were active across 20 sensorimotor events with a larger proportion of cells active during locomotion. Nevertheless, for any sensorimotor event, only about 17% cells were active comprising of conjunctive (C ∈ A and B) cells shared among events and complementary (C ∈ A not B or C ∈ B not A) cells active in individual events. Conjunctive cells identified similar sensorimotor events representing stable representations of familiar experiences and complementary cells suggested recruitment of new cells for encoding novel experiences. The moment-to-moment recruitment of complementary and conjunctive cells with changing sensorimotor events signifies the involvement of hippocampus in functional networks integrating sensory information with ongoing movement. This role of hippocampus is well suited for movement guidance, spatial behavior, episodic learning and memory, context representation and scene construction.

Introduction

The idea that the brain features behavior-specific electrographic events during the behavioral states of immobility and locomotion originated with the finding that electrical activity in the hippocampus is different during these two states (Kay and Frank, 2019; Vanderwolf, 1969). The electrical activity measured as local field potentials (LFPs) features large amplitude irregular activity

(LIA) during immobility and two kinds of rhythmical slow activity (RSA or theta activity, 6-12 Hz) that are sensory or movement related (Buzsáki, 2006; Buzsaki and Watson, 2012; Foster et al., 1989; Perentos et al., 2022; Vanderwolf, 1969; Whishaw, 1976; Whishaw and Vanderwolf, 1971, 1973). Sensory-induced RSA is cholinergic-dependent whereas movement-related RSA can be cholinergic-independent (Kramis et al., 1975; Vanderwolf et al., 1984; Whishaw and Dyck, 1984). The behavior-specific differentiation of electrical activity is also found at the cellular level. Whereas excitatory cells in both CA1 and CA2 modulate their firing in relation to location during immobility (Kay et al., 2016; Yu et al., 2017) and during locomotion (O'Keefe and Dostrovsky, 1971; O'Keefe and Nadel, 1978), anatomically distinct types of inhibitory cells fire preferentially during locomotion versus immobility (Arriaga and Han, 2017). There are reports of behavior-dependent cellular responses in the hippocampus when animals encounter sensory stimuli including odors (Igarashi et al., 2014; Komorowski et al., 2009; MacDonald et al., 2013; Manns et al., 2007; Taxidis et al., 2020), tones (Moita et al., 2003; Sakurai, 2002), tastes (Herzog et al., 2019), textures (Itskov et al., 2011), visual stimuli (Chen et al., 2013a; Zhao et al., 2020), and somatosensory stimuli (Bellistri et al., 2013; Wang et al., 2014).

These studies have not systematically investigated behavior-specific (immobile vs. locomoting) hippocampal cellular responses to sensory stimuli. Behavior-specific sensory processing is reported in sensory and non-sensory cortices, and some subcortical structures display behavior-dependent spontaneous and evoked firing activity - for a review, see (Schneider, 2020). Compared to immobility, locomotion increases firing of sensory neurons in the visual (Dipoppa et al., 2018; Niell and Stryker, 2010) and somatosensory (Ayaz et al., 2019; Sofroniew et al., 2015) cortices but reduces firing in the auditory cortex (Schneider et al., 2014). Locomotion also modulates higher order functions; for example, it improves sensory perception (Mineault et al., 2016), guides navigation through the visual cortex (Saleem et al., 2018), and alters the functional connectivity of visual and retrosplenial cortices

with other cortical regions (Clancy et al., 2019). Movements other than locomotion such as whisking, facial and body movements, and arousal-related changes in pupil diameter also influence neuronal firing properties in the sensory cortices (Musall et al., 2019; Stringer et al., 2019). Furthermore, movement-related inputs to the sensory cortices reflect expectations of sensory information anticipated by movements (Attinger et al., 2017; Keller et al., 2012). Although many studies have investigated hippocampal activity during spatial navigation and context processing [see reviews, (Colgin, 2020; Eichenbaum et al., 2016; Moser et al., 2017; Smith and Bulkin, 2014)], there has been no study explicitly comparing hippocampal cell population activity associated with immobility versus locomotion as is done here.

Calcium imaging was used to record hippocampal CA1 cell responses to sensory stimulation by a pressurized air stream or light flash while head-fixed mice were at rest or locomoting. A population level analysis investigated how cells were recruited during and between sensory stimuli applied during immobility versus locomotion. Subgroups of cells responding to different sensorimotor events were active in different stimulus-locomotion configurations. When two (or more) events were considered at a time, cells could be classified as complementary, responsive to only one event and conjunctive, responsive to both of events. From a large pool of responsive cells, complementary cells identified novel sensorimotor events and conjunctive cells encoded familiar sensorimotor events suggesting a recruitment with replacement organization.

Results

Experimental design, behavioral paradigm, and its characterization

Hippocampal CA1 cell activity was recorded from head-fixed mice resting or moving on a non-motorized conveyor belt (Fig. 1A). The application of a brake restricted movement and its release

enabled movement and running. An air stimulus delivered on the back and whole-field illumination with an LED in front of the mouse served as sensory stimuli. The behavioral paradigm featured 7 configurations of motor activity and sensory stimulation (Fig. 1B) divided into two sets based on two brake states: Brake (B) and No-Brake (NB). In Configurations 1, 2, 6, and 7, B-state prevented walk/run behaviors whereas in Configurations 3, 4, and 5, NB-state allowed walk/run behaviors. In Configurations 1 and 2, ten pulses each of light (L; 200 ms with 5 s interval) and air (A; 5 s with 10 s interval) were applied, respectively. In Configurations 3, 4, and 5, the air stream was applied to cause stimulus-induced running for a fixed distance of 150cm, one lap of the belt (before the air was stopped). Ten trials were given in each condition with an intertrial interval of 15 s. In Condition 4, a 200 ms light flash was also applied once the mouse had traveled 110 cm. Configurations 3 and 5, 1 and 6, and 2 and 7 were identical.

Neuronal activity 2 s before and 2 s after each stimulus event was analyzed and compared across B and NB states. For air stimuli, activity around both air onset and offset events (AOn and AOff respectively) was characterized whereas for light stimuli, activity at only light onset (L) was analyzed because of the brevity of stimulus duration i.e., 200 ms. Since hippocampus is an associative brain region, cellular activity may have resulted from intrinsic network activity representing task parameters or internal states. Therefore, the activity of cells was also analyzed around arbitrary (Arb) time points in which no sensory stimulation occurred in both B and NB states. The time chosen for Arb events (Fig. 1B, inset), was the mid-point of the intertrial intervals (in Configurations 2, 3, 4, 5, and 7). For B and NB states, the Arb point was 5 s and 7.5s after air offset respectively. Finally, during NB-state, activity of neurons was analyzed when animals voluntarily started or stopped their locomotion in the absence of sensory stimuli.

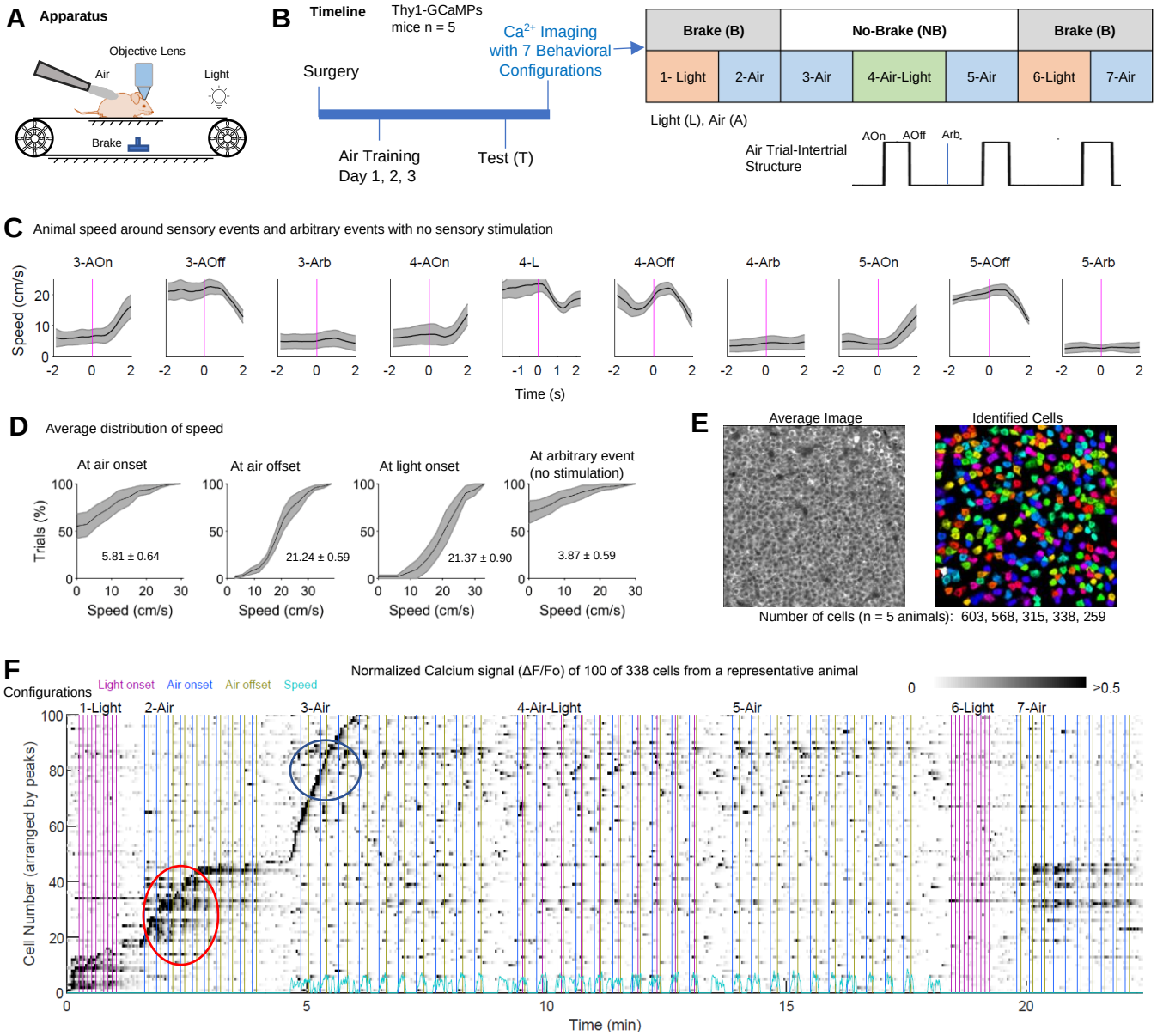

Figure 1. The experimental paradigm for studying hippocampal CA1 neuronal responses to sensory stimulation during immobility and locomotion. **(A)** Experimental setup. A head-fixed mouse on a linear conveyor belt receives a mild air stream on the back to motivate running. **(B)** Experiment timeline and list of 7 configurations that mice experienced while calcium imaging was performed. Inset shows schematic depicting air onset (AOn), air offset (AOff), and arbitrary (Arb) events. **(C)** Average speed over all trials by animals around stimulus and arbitrary (Arb) events during Configurations 3, 4, and 5. Magenta lines indicate occurrences of events. **(D)** Distribution of speeds at events mentioned in C. The numbers indicate overall mean±SEM speeds. **(E)** Average image (left) of the calcium imaging time series from a representative animal, and arbitrarily color-coded regions of interest indicating identified cell bodies (right) in a ~400 × 400 μm imaging window. **(F)** Normalized calcium traces ($\Delta F/F_0$), from 100 representative cells from a representative animal for a whole recording of ~25 min, overlayed with indicators of light and air stimuli (vertical-colored lines). The speed signal is shown at the bottom (cyan color). Notice differential firing of cells during immobility vs. locomotion (cells in blue vs red ovals). Thick black lines in (C) and (D) indicate mean over animals while shaded regions represent SEM.

The animals were mainly immobile during the B-state. During the NB-state, their average speed was always greater than zero around stimulus and Arb events (Fig. 1C). For AOff and L events, the speed in all trials (from Configurations 3-5) of individual animals was greater than zero (Fig. 1D, middle panels). For AOn, however, 50.00 ± 12.78 % of the trials on average (over 5 animals) had speeds greater than zero (Fig. 1D, left panel). There was animal-to-animal variability with greater than zero speeds in 3, 26, 18, 17, 11 trials (corresponding to 5 animals) of the cumulative 30 air application trials. In trials, in which the animals were immobile, they initiated locomotion after air onset with an average movement latency of 0.94 ± 0.06 sec (range: 0.05, 3.66, median: 0.62) and hence these trials were pooled with trials in which the mice were already moving at air onset. For the Arb events, there was animal-to-animal variability with greater than zero speeds in 2, 20, 21, 8, 6 trials (corresponding to 5 animals) of the cumulative 30 trials (Fig. 1D). Overall, however, the average speed around the Arb events was greater than zero (Fig. 1C).

Calcium imaging of the activity of hippocampal CA1 pyramidal neurons

Calcium imaging of CA1 pyramidal neurons was performed as the mice experienced the 7 behavioral configurations. Fig. 1E presents an average image of an imaging stack from a representative animal showing its densely packed dorsal CA1 neurons. Using Suite2p, a Python based analysis software, 603, 568, 315, 338, and 259 individual cells were identified from 5 mice (total: 2083 cells). An image of identified cells from a representative animal is displayed in Fig. 1E. The figure also shows that Suite2P did not recognize all visible cells in the average image, perhaps because some cells were seldom active (fired only occasionally). The raw calcium traces ($\Delta F/F_0$) of 100 cells from a representative animal shown in Fig. 1F demonstrate that cellular responses reflected brake states and/or sensorimotor

events. In one example, the cell groups colored red were active in the B-state and those colored blue were active in the NB-state. For further quantitative analysis of cellular responses to sensory events and behavior, as well as study of population level characteristics, the calcium signals were deconvolved to estimate firing rates for each cell. In the subsequent text, neural activity refers to the firing rates estimated from the calcium signals.

To examine the changes in cellular firing properties across B and NB states, mean and maximum firing rates were determined for both states and for each cell. The mean and maximum firing rates were then calculated to obtain the respective values for each animal. These values were then subjected to statistical comparison across states with a repeated measures analysis of variance (RM-ANOVA). The mean firing rate across B and NB states was not significantly different [0.054 ± 0.016 vs. 0.073 ± 0.022; F (1,4) = 7.05, p = .057, η^2 = .64], but note a higher mean for NB-state and a p value close to 0.05. The comparison of the maximum firing rates of cells for B and NB states gave a significant difference [26.47 ± 5.05 vs. 48.51 ± 10.14; F (1,4) = 13.89, p = .020, η^2 = .78] showing that locomotion contributed to increased transient cell firing.

Larger population of cells for No-Brake state vs Brake state for AOn, AOff, and Arb events

Cell activity during B and NB states for AOn, AOff, and Arb events was investigated by finding responsive cells and their response characteristics. Cells active around these events, were examined by generating raster plots of neuronal activity (trials versus time) for each cell and event. Peri-event time histograms (PETHs) were then calculated from raster plots by finding mean neuronal activity over trials. Responsive cells were identified from PETHs by statistically comparing average pre- and post- event firing rates using a Student's t-test (alpha < 0.05). This method allowed an unbiased approach for identifying both excited (Exc) and inhibited (Inh) cells in which post-event firing rates were either

significantly larger or smaller from their pre-event firing rates. Figure 2A displays raster plots for a representative AOn-Exc cell (left) and AOn-Inh cell (right) from the Configuration 2, with firing rates across time and across trials overlayed with the PETH. Population level response dynamics for responsive cells were observed with rate vector maps (Fig. 2B, top row). These show the normalized mean response of all cells organized by the time of each cell's peak response. The rate vector maps for both the B and NB states feature the binary nature of Exc and Inh cells (i.e., their responses of ON or OFF type) in relation to AOn. See the population correlation plots (Fig. 2B, middle row) in which each pixel represents a Pearson correlation between two columns of the corresponding rate vector map. Population correlations displayed dark square-like regions for both the pre-event (-2 to 0 s) and post-event (0 to 2 s) periods corresponding to responses of Exc and Inh cells, respectively. Plots of the average population correlation (Fig. 2B, bottom row) confirmed that the majority of Exc and Inh cells were binary in nature. Plots generated for AOff and Arb events exhibited similar characteristics with both Exc and Inh cells.

To assess the magnitude of cell activation across B and NB states, responsivity (Resp), the percent of activated cells (including both Exc and Inh cells) around AOn, AOff, and Arb events was found. Resp was averaged over Configurations 2 and 7, and Configurations 3, 4, and 5 for B and NB states, respectively. The data were subject to a two within-subjects factors (Brake-State and Event-Type) RM-ANOVA. There were significant main effects of both Brake-State [F (1,4) = 130.12, $p < .001$, η^2 = .97] and Event-Type [F (2,8) = 19.22, $p = .009$, $\eta^2 = .83$] with no interaction. The Resp in the NB-state was larger than in the B-state and post hoc comparisons revealed that the percent of cells activated around AOn was larger than for AOff and Arb events (Fig. 2C).

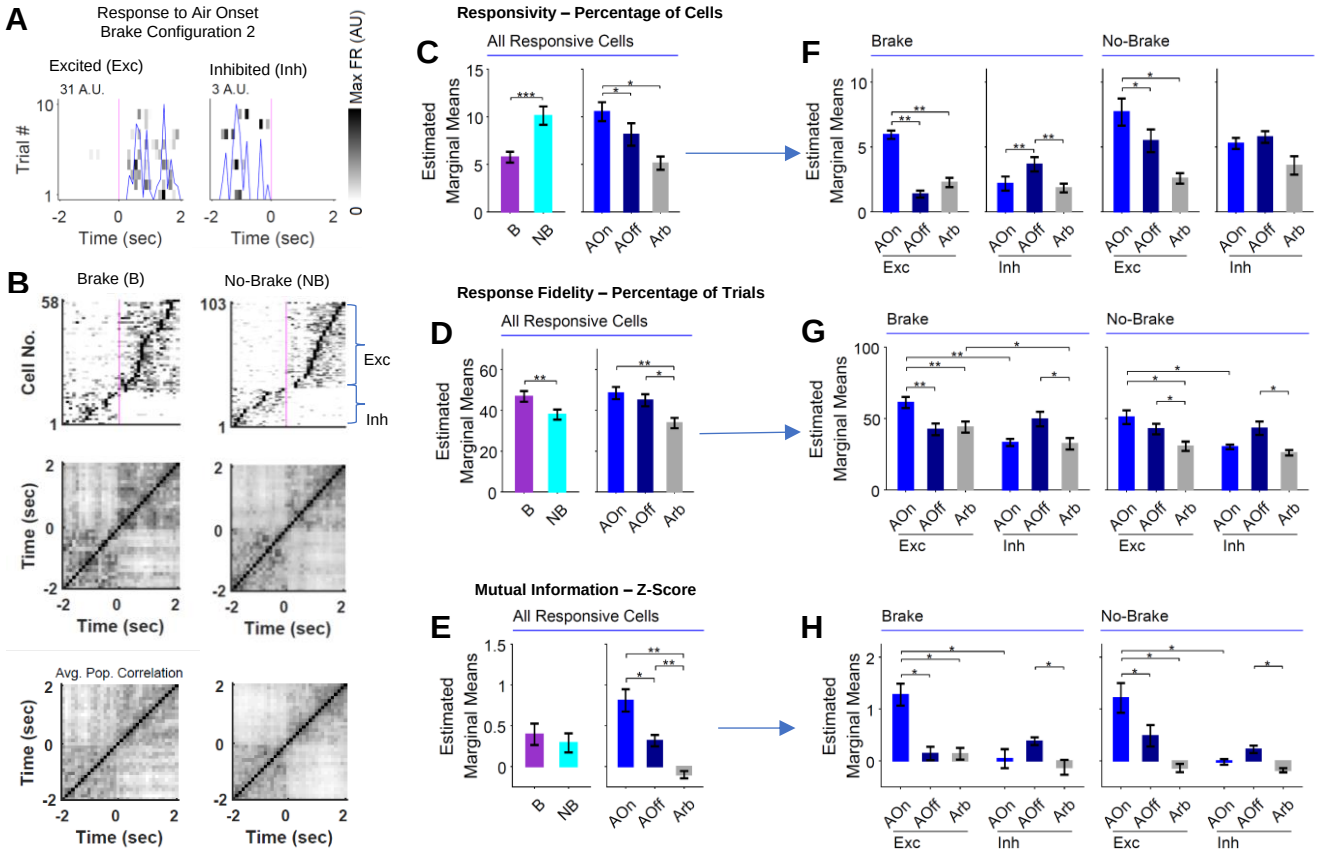

Figure 2. More cells active during No-Brake compared to Brake State for AOn, AOff, and Arb events. **(A)** Raster plots of representative excited (Exc) and inhibited (Inh) cells showing increased and decreased firing, respectively, in response to AOn (t = 0, magenta line). The blue lines show the means across trials. **(B)** Rate vector maps (top row) and corresponding population vector correlation plots (middle row) of responsive cells from a representative animal for Brake vs. No-Brake states. Average population correlation plots (bottom row) from 5 animals. **(C-E)** Results of two-way RM-ANOVA for assessing responsivity (Resp), response fidelity (RF), and mutual information z-score (zMI) respectively, across brake states (B versus NB) and events (Aon, AOff, and Arb) **(F-H)** Results of three-way RM-ANOVA for assessing Resp, RF, and zMI respectively, across brake states, events, and cell types (Exc vs Inh). For all statistical tests, n = 5 mice. Error bars = SEM. *p < .05, **p < .01, ***p < .001.

Responsive cells found from PETHs might have had different response characteristics across trials during B and NB states in response to AOn, AOff, and Arb events. Therefore, two measures, response fidelity (RF) and mutual information (MI) were extracted from raster plots to quantitatively assess the strength and robustness of responses across trials. RF was defined as percent of trials in which the cell's firing rate was greater than zero at any point during a trial. MI between firing rate and time

was determined from a raster plot (Souza et al., 2018) and then z-scored (zMI) using a distribution of 500 MI values calculated from randomly shuffled instances of the same raster plot. A larger zMI value indicates better/tighter temporal repeatability of response across trials. RF and zMI values were averaged across Configurations 2, 7, and Configurations 3, 4, and 5, for B and NB states, respectively. The results were subject to a two within-subjects factors (Brake-State and Event-Type) RM-ANOVA individually for RF and zMI. For RF, there were significant main effects of both Brake-State [F (1,4) = 41.32, p = .003, η^2 = .91] and Event-Type [F (2,8) = 30.62, p = .000, η^2 = .88] with no interaction. RF in the B-state was larger compared to the NB-state and post hoc comparisons revealed that the RF for AOn and AOff was larger compared to Arb events (Fig. 2D). For zMI, there was a main effect of Event-Type [F (2,8) = 42.50, p = .001, η^2 = .91] with post hoc comparisons showing that zMI for AOn and AOff events was larger compared to Arb events and that for AOn was larger compared to AOff (Fig. 2E).

Taken together the results suggest that more cells are active during NB-state compared to B-state. Nevertheless, cells that were active during B-state had more robust responses than occurred for cells active during the NB-state. Additionally, cells that were activated by sensory air events had a more robust response compared to those activated around Arb events, especially at AOn.

Characteristics of excited and inhibited cells similar across Brake and No-Brake states but different for AOn and AOff events

The analysis of cell populations activated across B and NB states around AOn, AOff, and Arb events was further extended to ask how Brake-State and Event-Type might have invoked different cell types (Exc and Inh cells). A three within-subjects factors (Brake-State, Event-Type, and Cell-Type) RM-ANOVA was used on the output variables: Resp, RF, and zMI.

For Resp, there was a significant three-way interaction, [F (2,8) = 6.73, p = .028, η^2 = .63]. Therefore, simple two-way interactions of two factors at each level of the third factor were assessed with a Bonferroni adjusted alpha value (see methods). Significant simple two-way interactions were found between Event-Type and Cell-Type for both Brake [F (2,8) = 51.37, p < .001, η^2 = .93] and NB-state [F (2,8) = 9.14, p = .010, η^2 = .70]. In the next level of analysis, simple simple main effects were assessed with a Bonferroni adjusted alpha value. Only simple simple main effects of Event-Type were significant: B-state, Exc cells [F (2,8) = 56.15, p < .001, η^2 = .93], Inh cells [F (2,8) = 32.19, p < .001, η^2 = .89], and NB-state, Exc cells [F (2,8) = 12.98, p = .003, η^2 = .76]. Simple simple comparisons with Bonferroni correction then assessed differences in means for Event-Types (Fig. 2F). The effect of AOn was stronger in generating Exc responses for both B and NB states, but AOff was more potent in generating Inh responses only for B-state although the trend was similar for NB-state.

For RF, there was a main effect of Brake-State [F (1,4) = 32.21, p = .005, η^2 = .89] and a two-way interaction between Event-Type and Cell-Type [F (2,8) = 25.50, p = .006, η^2 = .86]. Posthoc comparisons (Fig. 2G) showed that Exc and Inh cells activated around AOn and AOff respectively had the largest RF in both B and NB states. For zMI, there was a significant two-way interaction between Event-Type and Cell-Type [F (2,8) = 21.26, p = .004, η^2 = .84]. Post hoc comparisons revealed larger zMI values for AOn-Exc cells and AOff-Inh cells (Fig. 2H).

Taken together, the results suggest that Exc and Inh cells were similar in the B and NB states, but AOn was associated with more Exc cells and AOff was associated with more Inh cells. As found before, sensory air events generated more robust responses compared to Arb events for both Exc and Inh cells.

Separate groups of cells in Brake and No-Brake states for AOn, AOff, and Arb events

The population level activity of cells was classified across brake states and different events as conjunctive and complementary. Considering two cellular populations active around two sensorimotor events e.g., A and B, conjunctive (Conj) cells were defined as those active for both events (Conj ∈ A and B) and two types of complementary (Comp) cells were defined as those active for individual events (Comp1 ∈ A not B; and Comp2 ∈ B not A). The percent of these three cell populations (of the total number of cells) for different sensorimotor events was compared statistically or with a secondary level of analysis to observe relations among sensorimotor events and configurations.

Comp1, Conj, and Comp2 cell populations were found for AOn, AOff, and Arb events where Comp1 and Comp2 were selectively active during B and NB states respectively and Conj were active in both. For this analysis, cells were pooled across Configurations 2, 7 and Configurations 3, 4, 5 for B and NB states, respectively. Percent of populations were then subjected to a two-way RM-ANOVA with Event-Type and Population-Type as within-subjects factors. There was significant main effect of both factors, Event-Type [F (2,8) = 10.53, p = .030, η^2 = .72] and Population-Type [F (2,8) = 715.73, p < .001, η^2 = .99] but no significant interaction. The former result was expected as described above about differences in Resp across sensory air and Arb events (Fig. 2C and Fig. 3A). The later result however showed differences in percent across population types with Conj cells having a significantly smaller population compared to Comp1 and Comp2 identified with post hoc comparisons (Fig. 3A).

The complementation and conjunction of Exc and Inh cells was then examined by extending the analysis by adding a third factor (Cell-Type) and performing a three-way RM-ANOVA. There was a significant three-way interaction [F (4,16) = 7.19, p = .002, η^2 = .64]. Further tests showed that the only simple two-way interaction was between Cell-Type and Event-Type for Comp1 type of cells [F (2,8) = 20.68, p = .003, η^2 = .84]. Simple simple main effects of both Cell-Type and Event-Type were

significant: [F (2,8) = 12.88, p = .003, η^2 = .76] and [F (2,8) = 11.31, p = .005, η^2 = .74], respectively. Post hoc comparisons showed that for Exc cells, AOn had a larger percentage compared to AOff and the opposite was true for Inh cells (Fig. 3B). For Conj and Comp2 cells, there was no difference across Exc and Inh cell types (Fig. 3B, pooled data).

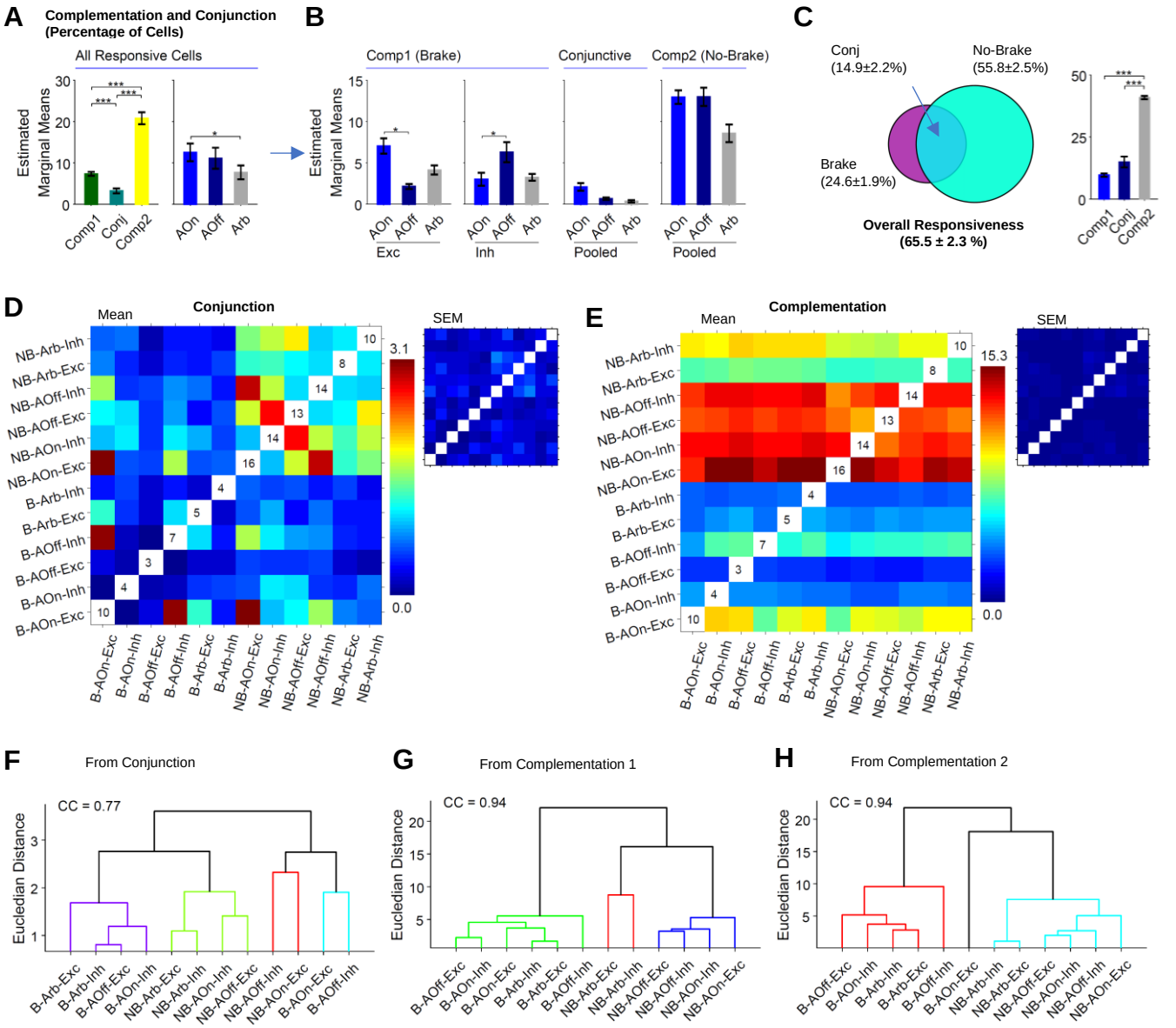

Figure 3. Segregated cell populations in Brake and No-Brake states for AOn, AOff, and Arb events. **(A)** Results of a two-way RM-ANOVA for assessing the percent of cells across population types (Comp1, Comp2, and conjunctive) and events (AOn, AOff, and Arb). **(B)** Results of a three-way RM-ANOVA assessing the percent of cells across cell types (Exc vs Inh) in addition to factors in (A). **(C)** Overall responsivity, conjunction, and complementation across Brake and No-Brake states. **(D-E)** Average and SEM (insets) heatmaps (over 5 animals) of conjunction and complementation of Exc and Inh cell groups

active in Brake and No-Brake states around AOn, AOff, and Arb events. **(F-H)** Dendrograms resulting from agglomerative hierarchical clustering of the average conjunction and complementation heatmaps/matrices. CC indicates cophenetic correlation. For all statistical tests, $n = 5$ mice. Error bars = SEM. *$p < .05$, **$p < .01$, ***$p < .001$.

When pooled across event and cell types, there were overall 65.5 ± 2.3 % responsive cells with one population active during the B-state (Comp 1, 9.7 ± 0.7 %), one population active during the NB-state (Comp 2, 40.9 ± 0.6 %) and one population active in both conditions (Conj, 14.9 ± 2.2 %) (see Fig. 3C, Venn Diagram). After pooling however, the average percentage of Comp1 cells was not significantly different from the average percentage of Conj cells (Fig. 3C, RM-ANOVA and post hoc comparison), which suggests that some cells might have shared responsiveness across sensory air and Arb events. To further investigate this, the conjunction and complementation of all different groups of cells was analyzed. The conjunction and complementation of different groups of cells categorized by brake states (B vs NB), event types (AOn, AOff, and Arb) as well as cell types (Exc vs Inh) were plotted as heat maps. Figures 3D and 3E show average conjunction and complementation heatmaps respectively (over 5 animals) and insets show SEM heatmaps. In the average heatmaps, diagonal pixels are shown as white with no color coding and numbers therein represents the percentage of responsive cells for the selected category. Off-Diagonal pixels in these heatmaps show percentages of conjunctive and complementary cells. For the complementation heatmap, pixels above and below the diagonal represent Comp1 and Comp2 cells, respectively when considering row-column pairs.

Conjunctive cell populations were small, with ~3 % conjunction between Exc cells responsive to AOn and Inh cells responsive to AOff during the Brake conditions (Fig. 3D, B-AOn-Exc vs B-AOff-Inh, row 1 column 4). To find overall classification of cell populations and their relationships with each other, a secondary analysis with agglomerative hierarchical clustering (see methods) of the average heatmap matrix was used. Clustering revealed four distinct clusters (Fig. 3F). The cyan cluster grouped

Exc cells responding to AOn with Inh cells responding to AOff during the B-state indicating cells that responded during air ON periods i.e., when air was present. A similar relation existed for the same types of cells and events during the NB-state (red cluster). The third cluster constituted cells from the B-state (purple cluster), which were active during air OFF periods i.e., when air was not present. The fourth cluster (green) represented air OFF cells for the NB-state. These results show that conjunctive cells across sensory air and Arb events could be segregated into two groups for the B and NB states, and further subdivided into cells that responded to air ON and OFF periods.

The complementation heatmap showed segregation between B and NB states with a largest complementation between NB-AOn-Exc and B-AOff-Exc cell groups (~15.3 %). The complementation heatmap was split into two heatmaps, symmetric across the diagonal, by using the upper and lower triangular matrices corresponding to Comp1 and Comp2 cells. The clustering of Comp1 heatmap (Fig. 3G) showed separate grouping of cells across B (green cluster) and NB (blue and red clusters) states. The clustering of Comp2 (Fig. 3H) showed similar cluster segregation of B and NB states (cyan and red clusters, respectively). However, within the dendrograms event-cell-type combinations, grouping mainly occurred based on event-type e.g., NB-AOff-Exc closer to NB-AOff-Inh and NB-AOn-Exc closer to NB-AOn-Inh. Taken together, the results show segregation of cell groups across B and NB states when cells were divided into subgroups based on AOn, AOff, and Arb events and cell types.

Separate groups of cells for Light-onset in Brake and No-Brake states

Light-onset cell populations were analyzed to investigate whether same or different cellular networks might be involved across B and NB states. The above-mentioned analysis (for AOn, AOff, and Arb events) was repeated for cell populations active around light stimulus events in Configurations 1 and 4 for B and NB states respectively. Both Exc and Inh cells were found in a similar way as explained

above. Fig. 4A shows raster plots and peri-event histograms (PETHs) for representative Exc and Inh cells from Configuration 1. Rate vector maps (Fig. 4B, top row) and population vector correlation plots (Fig. 4B, middle and bottom rows) showed the binary nature of cellular responses for both representative populations in the B and NB states.

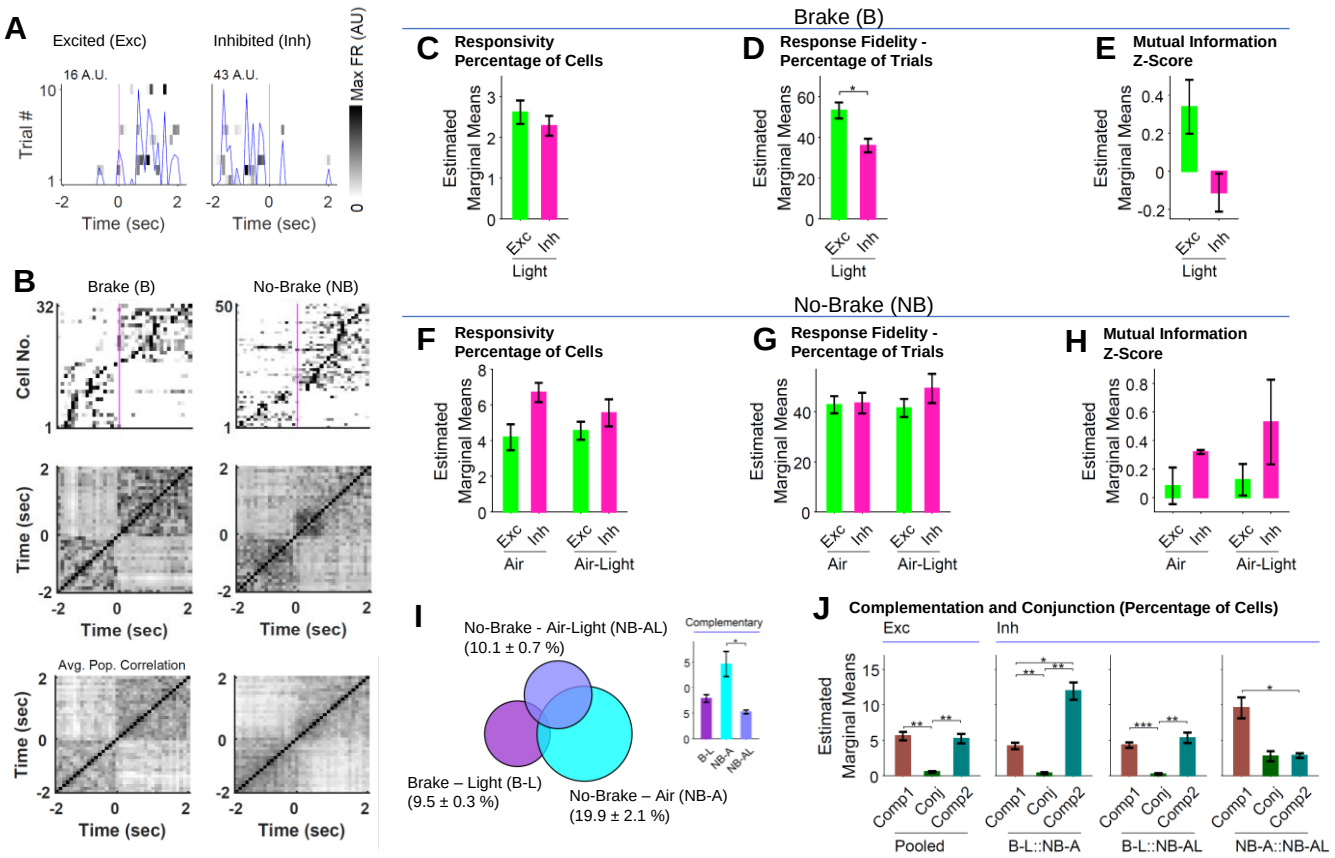

Figure 4. Segregated cell populations across Brake and No-Brake states to a light stimulus. **(A)** Raster plots of representative Exc and Inh cells. The magenta line at t = 0 indicates light onset. The blue lines show means over trials. **(B)** Rate vector maps (top row) and corresponding population vector correlation plots (middle row) of responsive cells from a representative animal for Brake and No-Brake states. Average population correlation plots (bottom row) from 5 animals. **(C-E)** Results of one-way RM-ANOVA assessing responsiveness, response fidelity, and mutual information z-score of Exc and Inh cells for light stimulus in Brake state (B-L). **(F-H)** Results of two-way RM-ANOVA assessing response variables for Exc and Inh cells in the No-Brake state for light stimulus combined with air (NB-AL) and identical Arb event where only air was present (NB-A). **(I)** Overall responsivity, conjunction, and complementation for B-L, NB-AL, and NB-A cell populations. **(J)** Results of three-way RM-ANOVA for assessing the percent of cells across population types (Comp1, Comp2, and Conj), cell types (Exc vs Inh) and event pairs e.g., B-L::NB-AL. For all statistical tests, $n = 5$ mice. Error bars = SEM. *$p < .05$, **$p < .01$, ***$p < .001$.

The Resp, RF, and zMI were separately assessed for B and NB states because only light stimulus was applied in B-state (B-L) but for NB-state, light was applied while the air was ON (NB-AL, Air-Light). For B-state, values were averaged from Configurations 1 and 6. There was no significant difference between Exc and Inh cells for Resp and zMI values but RF of Exc cells was larger than that of Inh Cells [F (1,4) = 9.85, p = .035, η^2 = .71] (Fig. 4C-E). For NB-state, NB-AL cell population from Condition 4 was compared with cells active for identical Arb events in Configurations 3 and 5 where only air was being applied with no light stimulation (NB-A, Air). A two-way RM-ANOVA with Cell-Type (Exc and Inh) and Event-Type (A and AL) as within-subjects factors was used and none of the main or interaction effects were significant for any of the variables (Fig. 4F-H).

Cell populations corresponding to the three sensorimotor events, B-L, NB-A, and NB-AL were then compared for complementation when taken collectively and pooled across Exc and Inh cell types (Fig. 4J). There were separate groups of cells active around the three events with NB-A having the largest percentage of complementary cells (tested with RM-ANOVA with Event-Type as within-subjects factor) [F (2,8) = 8.99, p = .009, η^2 = .69]. When taken two at a time, a three-way RM-ANOVA was conducted with Event-Type-Pair e.g., B-L::NB-AL, Population-Type (Comp1, Conj, and Comp2), and Cell-Type (Exc and Inh) as within-subjects factors. There was a significant three-way interaction [F (4,16) = 5.83, p = .004, η^2 = .59]. Simple two-way interactions were then examined, and the only difference was between Event-Type-Pair and Population-Type for Inh cells [F (4,16) = 16.71, p = .005, η^2 = .81]. Simple simple main effects of Population-Type were then individually determined for all Event-Type-Pairs and all were significant: B-L::NB-A [F (2,8) = 54.13, p < .001, η^2 = .93], B-L::NB-AL [F (2,8) = 41.41, p < .001, η^2 = .91], and NB-A::NB-AL [F (2,8) = 12.12, p = .004, η^2 = .75]. Post hoc comparisons revealed that for the first two Event-Type-Pairs involving B and NB states, there were more complementary cells than conjunctive cells, but was not the case for the third Event-Type-Pair

involving events in only NB-state (Fig. 4J). The percent of complementary Exc cells was significantly larger than the percent of conjunctive cells (Fig. 4J) for all Event-Type-Pairs. These results suggest a segregation of cell populations across B and NB states for both Exc and Inh cells active around light stimuli that are additionally different from the cells active around only-air-Arb (A) event.

Separate groups of cells active for distinct sensorimotor events

The dynamics of the recruitment of cells across different sensorimotor events in all behavioral configurations was analyzed by finding the conjunction and complementation of cell populations active around all sensory and Arb events after pooling across Exc and Inh cell types (Fig. 5A-B). Agglomerative hierarchical clustering of the average heatmaps was then used to identify relationships among conditions (Fig. 5C-E). The clustering analysis showed a segregation of cellular populations across B and NB states either with clear clustering or branch separation in dendrograms within the same clusters. However, there was some mixing of populations across B and NB states for Arb events.

The clustering from the conjunction heatmap (Fig. 5C) revealed that distinct subgroups of cells were active for distinct sensorimotor events. For example, the blue cluster shows the closeness of cells active around AOn in NB-state (Configurations 3, 4, and 5). Similar relationship exists for B-state (Configurations 2 and 7), see dendrogram branch in red cluster enclosed with dotted blue line. The green cluster represents cells active around AOff in NB-state and the branch in red cluster enclosed with dotted green line represents similar cells for B-state. The branch indicated with magenta arrowhead shows the closeness of populations active around light in B-state (Configurations 1 and 6). The cell populations active around Arb events in NB-state (3-Arb, 4-Arb, and 5-Arb) however, were closer to cell populations active in B-state. When the Arb, A, and A-L events were excluded from clustering,

more distinct grouping of cell populations occurred which were active for distinct sensorimotor events (Fig. 5F) and there was clear separation between B and NB states.

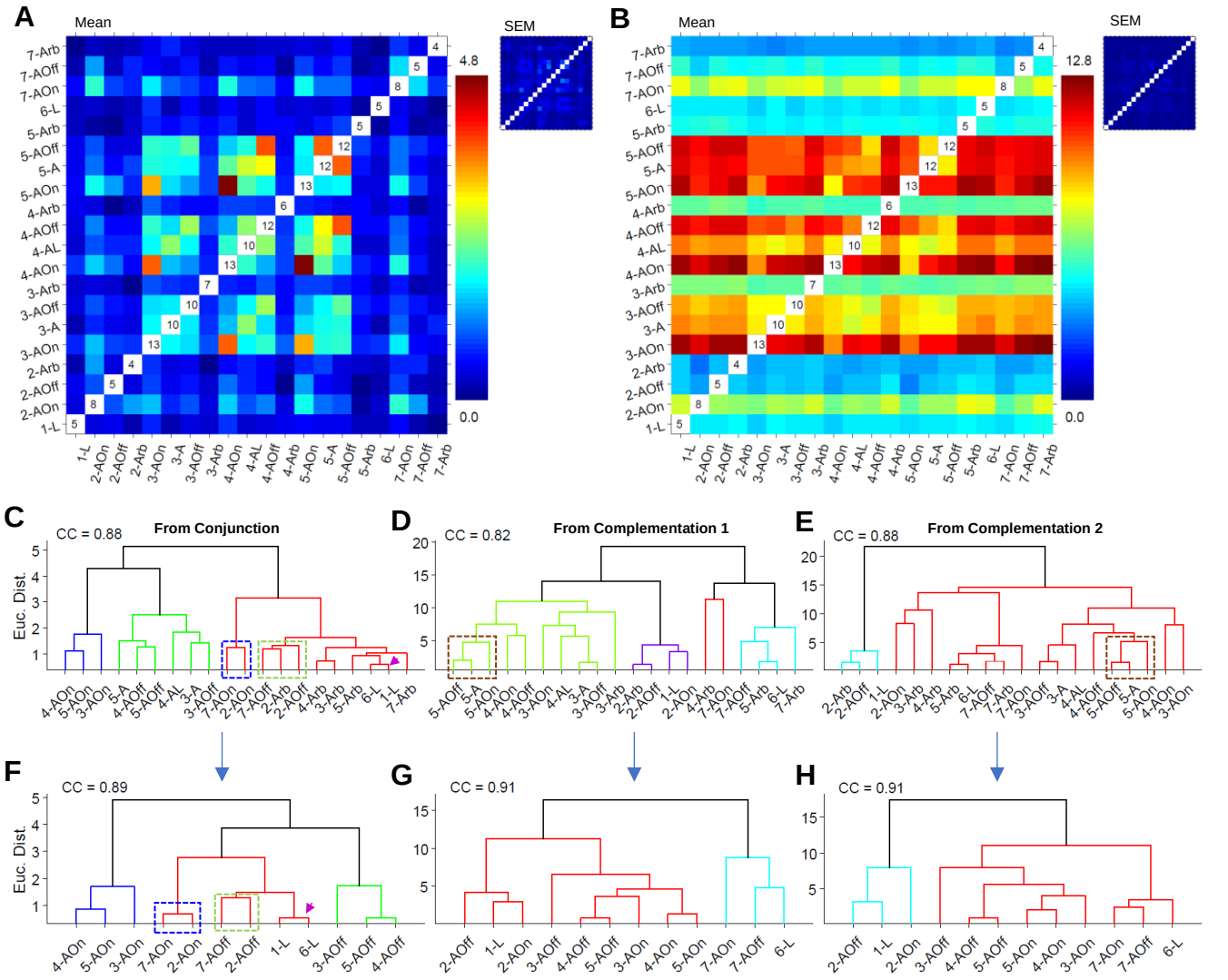

Figure 5. Separate subgroups of cells are active for distinct sensorimotor events. **(A-B)** Average and SEM (insets) heatmaps (over 5 animals) of conjunction and complementation of cell groups active in Brake and No-Brake states around sensory air, light, and Arb events. **(C-E)** Dendrograms resulting from agglomerative hierarchical clustering of the average conjunction and complementation heatmaps/matrices. **(F-H)** Dendrograms resulting from agglomerative hierarchical clustering of the average conjunction and complementation heatmaps/matrices after excluding arbitrary events. CC indicates cophenetic correlation.

The clustering of both complementation heatmaps (Fig. 5D-E) revealed grouping of sensorimotor events that either belonged to the same Configuration or those that happened close in time.

For example, in the purple and cyan clusters in Figures 5D and 5E respectively, 1-L was grouped with 2-AOff and 2-Arb events (for B-state). Similarly, the green cluster in Figure 5D shows grouping of sensorimotor events in NB-state with branch proximity of sensorimotor events belonging to the same Configuration e.g., 5-AOff, 5-A, 5-Aon enclosed with dotted brown line. The cyan cluster in Fig. 5D shows grouping of events in Configurations 6 and 7 with 5-Arb event from NB-state. In both heatmaps for complementation, if Arb, A, and A-L events were excluded, a clear separation between B and NB states was seen and within branches, grouping of sensorimotor events occurred based on one Configuration or Configurations that occurred close in time (Fig. 5G-H).

The conjunction and complementation of the above-mentioned populations was also studied with cells that responded around voluntary motion onset and offset events when there was no sensory stimulation. During the no stimulus intervals of the NB-state, animals sometimes walked or ran spontaneously. These events were identified and subdivided into components in which an animal started locomoting (motion onset, MOn) or stopped locomoting (motion offset, MOff). For 5 animals, the number of MOn events detected was 8, 21, 19, 20, and 19, and the number of MOff events was 35, 24, 31, 37, and 39. Cellular activity around these events (1.5 s pre- and post-event) was assessed by generating raster plots and PETHs to identify voluntary motion-related cellular responses. Both Exc and Inh cell responses (Fig. 6A) were identified. Rate vector maps (Fig. 6B, top row) and population correlation plots (Fig. 6B, middle and bottom rows) showed the binary nature of the responses. The effect of Event-Type (MOn vs. MOff) and Cell-Type (Exc vs. Inh) on the percentages of responsive cells was examined with a RM-ANOVA. There was a significant interaction effect [F (1,4) = 45.73, p = .002, η^2 = .92], with a greater number of cells showing an Exc than an Inh response to MOn (p = .025), and vice versa for MOff (p = .002) (Fig. 6C). The same analysis for response fidelity revealed a significant effect of Event-Type (Fig. 6D) [F (1,4) = 8.12, p = .046, η^2 = .67]. The fidelity of the cells

responding to MOn was significantly greater than that of the cells responding to MOff. There was no significant main effect or interaction between factors for zMI values (Fig. 6E). These results suggest more cells responded during locomotion with a more robust response to MOn.

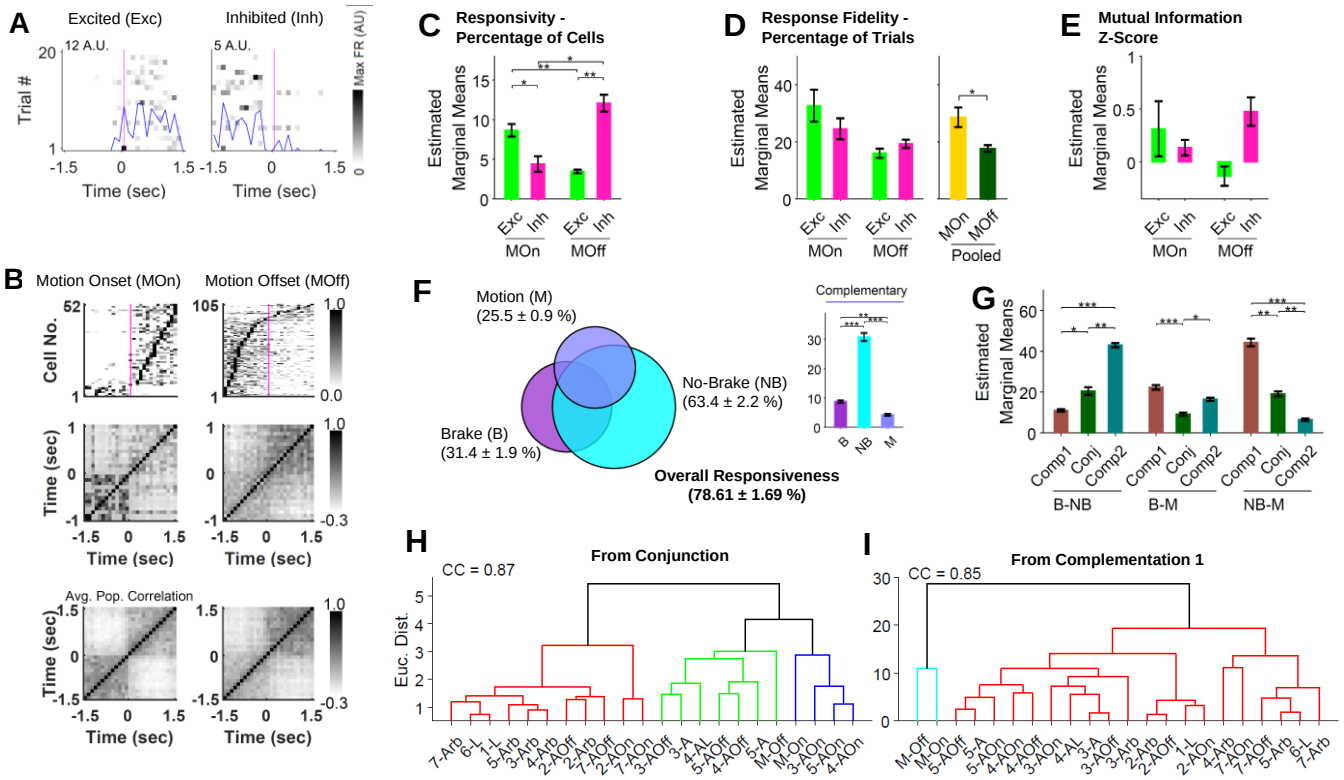

Figure 6. Separate cell groups at movement onset (MOn) and offset (MOff) events compared to other sensorimotor events. **(A)** Raster plots of representative Exc and Inh cells to MOn. The magenta line at t = 0 indicates motion onset. The blue lines show means over trials. **(B)** Rate vector maps (top row) and corresponding population vector correlation plots (middle row) of responsive cells from a representative animal for MOn and MOff events. Average population correlation plots (bottom row) for 5 animals. **(C-E)** Results of two-way RM-ANOVA for assessing responsivity, response fidelity, and mutual information z-score for MOn vs. MOff and Exc vs. Inh cells. **(F)** Overall responsivity, conjunction, and complementation for Brake, No-Brake, and Motion conditions. **(G)** Results of two-way RM-ANOVA for assessing the percent of cells across population types (Comp1, Conj, and Comp2) and condition pairs e.g., Brake and Motion (B-M). **(H-I)** Dendrograms resulting from agglomerative hierarchical clustering of the average conjunction and complementation heatmaps/matrices when MOn and MOff events were included. CC indicates cophenetic correlation. For all statistical tests, $n = 5$ mice. Error bars = SEM. *$p < .05$, **$p < .01$.

To examine whether cells exhibiting responses to MOn and Moff (M-condition) responded to events during the B-state (B-condition) and non-voluntary motion events in the NB-state (NB-

condition), cells were pooled across events (AOn, AOff, Arb, L, A, and A-L), response types (Exc vs. Inh), and stimulus types (air and light). Overall, there were 78.61 ± 1.69 % responsive cells with 8.8 ± 0.4 %, 30.8 ± 1.4 %, and 4.2 ± 0.3 % active in B-, NB-, and M- conditions, respectively and 6.9 ± 0.9% responding during all three conditions (Fig. 6F). When taken collectively, the percentage of complementary cells in the NB-condition was significantly larger than in the B and M conditions (p < .001 for both comparisons) whereas the percentage in the B-condition was larger than that in M-condition (p = .003): (Fig. 6F) [RM-ANOVA, F (2,8) = 210.72, p < .001, η^2 = .98]. When taken two at a time, percent of complementary and conjunctive cells were compared by using a two-way RM-ANOVA with Condition-Pair e.g., B-M, NB-M, and Population-Type (Conj, Comp1, and Comp2) as within-subjects factors. There was a significant interaction between the two factors [F (4,16) = 210.78, p < .001, η^2 = .98]. Post hoc comparisons revealed that for the B-M comparison, the percentage of conjunctive cells was significantly smaller than complementary cells (Fig. 6G, p = .012 and p < .001). However, there was a larger overlap of cells between NB and M conditions with a larger percentage of complementary cells in NB-condition (Fig. 6G, p = .001, .0003, and .0047).

The conjunction and complementation of cells responding to MOn and MOff events was also analyzed with all other sensorimotor events in B and NB states. Cell populations for MOn and MOff were closer to AOn and AOff events respectively in NB-state revealed from clustering of conjunction heatmap (Fig. 6H). The clustering of complementation heatmaps showed that MOn and MOff formed a separate cluster which suggested that the complementary cells related to voluntary motion were distinct compared to other cell populations.

Taken together, these results suggest that there were separate cell populations which were active for distinct sensorimotor events in different behavioral configurations. Where the conjunctive cell populations indicated stable cellular representations, complementary cell populations showed the

dynamics of recruitment across different sensorimotor events which was analyzed next by doing a trial-by-trial analyses of the activity of cells.

Trial-wise turnover of cellular recruitment reveals larger percentage of complementary cells for No-Brake state and early compared to later trials

To examine how cells were recruited during individual trials of presentations of air and light stimuli and arbitrary events during the B and NB states, responsive cells (firing rate > 0) were identified for each trial. The percentages of responsive cells in each trial were found for the 20 different sensorimotor events mentioned in the previous sections (see Fig. 7A). Overall, on average, 17.3 ± 0.1% (range: 13.07, 23.02, median: 17.34) of cells were responsive in any given event (Fig. 7A, magenta line). Across all trials for all events, 99.7 ± 0.1% of cells were responsive. To statistically compare the percent of responsive cells across the 20 events and 10 trials, a two-way RM-ANOVA was used. There was a significant effect of Event-Type on the percent of responsive cells (Fig. 7C), [F (19,76) = 2.10, p = .012, η^2 = .34]. Post hoc comparisons revealed differences in means for a few events (Fig. 7C). Consistent with previous observations, a larger percentage of cells responded to sensory stimuli during the NB-state and with an abrupt increase in the percent of cells at Brake to No-Brake transition in Configuration 3.

The dynamics of the percent of complementary and conjunctive cells was also assessed by considering adjacent pairs of trials (trials 1 and 2, trials 2 and 3, etc.). For the 9 pairs of trials for each of the 20 events, Conj, Comp1, and Comp2 cells were identified (Fig. 7B). Where Conj cells were active in both trials in a trial-pair, Comp1 cells were active in the former trial but became silent in the later trial, and Comp2 cells started silent but became active in the later trial.

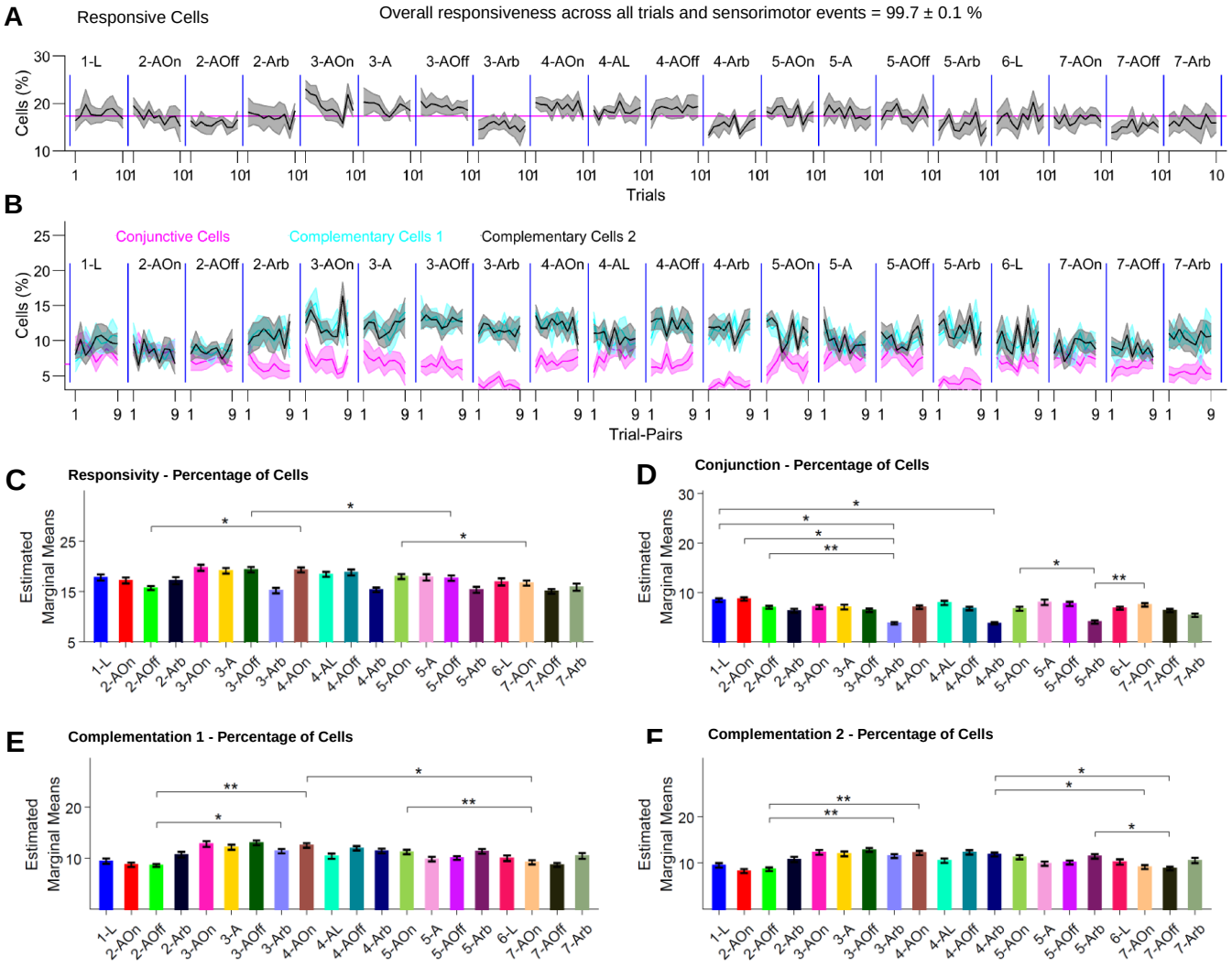

Figure 7. Adjacent trial-wise dynamics of cellular responses and conjunction/complementation in cellular populations reveals larger complementation in No-Brake state and early trials. **(A)** Percent of responsive cells (firing rate > 0) over trials for 20 types of cellular responses to different sensorimotor events exhibited across the 7 behavioral configurations. **(B)** Percent of complementary and conjunctive cells for pairs of adjacent trials. Pairs 1-9 correspond to Trials 1-2, 2-3, 3-4, etc. up to 9-10. **(C)** Result of two-way RM-ANOVA assessing responsivity across 20 events and 10 trials. **(D-F)** Results of two-way RM-ANOVA assessing the percent of conjunction and complementation across 20 events and 9 trial-pairs. For all statistical tests, $n = 5$ mice. Error bars = SEM. *$p < .05$, **$p < .01$.

A two-way RM-ANOVA with Event-Type and Trial-Pairs as within-subjects factors of the percent of Conj cells gave a significant effect of Event-Type [F (19,76) = 5.87, $p < 0.001$, $\eta^2 = .59$]. Post hoc tests revealed significantly smaller percentages during Arb events (Fig. 7D, see significant post hoc comparisons). Similar analysis on the percent of complementary cells showed that percent of both

Comp1 and Comp2 cells were significantly different across Event-Types: [F (19,76) = 2.81, $p < 0.001$, $\eta^2 = .41$] and [F (19,76) = 2.82, $p < 0.001$, $\eta^2 = .41$. Post hoc comparisons revealed a larger percent of both types during NB-state compared to B-state (Fig. 7E-F, see significant post hoc comparisons). The percent of Comp2 cells were also different across trial-pairs [F (8,32) = 2.41, $p = .037$, $\eta^2 = .38$]. Post hoc comparisons did not show any differences in means across trial-pairs. However, if only air and light stimuli were considered, the percent of Comp2 cells was significantly different across events [F (12,48) = 3.79, $p = .0005$, $\eta^2 = .49$] as well as trial-pairs [F (8,32) = 2.76, $p = .019$, $\eta^2 = .41$] with trial-pair 1-2 having a larger percentage of cells compared to trial-pair 9-10 (post hoc comparison, $p = .021$). These results suggest locomotion contributing to more new cells being recruited immediately following a new event (experience).

The conjunction and complementation of cells for all trial-pairs (200 × 200) corresponding to 20 events and 10 trials were qualitatively assessed with heatmaps. The average heat maps for conjunctive and complementary cells are shown in Fig. 8. The heatmap of conjunctive cells (Fig. 8A) shows that there are separate subgroups of cells that are selectively active during different events. For example, see the checkerboard-like pattern in the middle of the map outlined by thick brown box, which shows that separate subgroups of cells respond to AOn versus AOff (outlined with red boxes). Furthermore, some of the cells that participated during the first B-state also did so selectively during the second B-state (outlined with purple boxes). Cells that responded to light during the NB-state had a high overlap with cells that responded to AOff during the NB-state. To perform clustering on the conjunction heatmap, it was binned to average across trial-pairs i.e., all 100 pixels corresponding to 10 x 10 trial-pairs within each big black box were averaged. This way an average heatmap was obtained and subjected to agglomerative hierarchical clustering. It showed that there was a clear segregation within the dendrograms for B versus NB states (Fig. 8C, dotted green box versus other branches). Further

segregation on branch level can be seen for grouping of sensory and arbitrary events (blue and purple dotted boxes and cyan cluster). The segregation between B and NB states was clearer when Arb and A events were excluded (Fig. 8F).

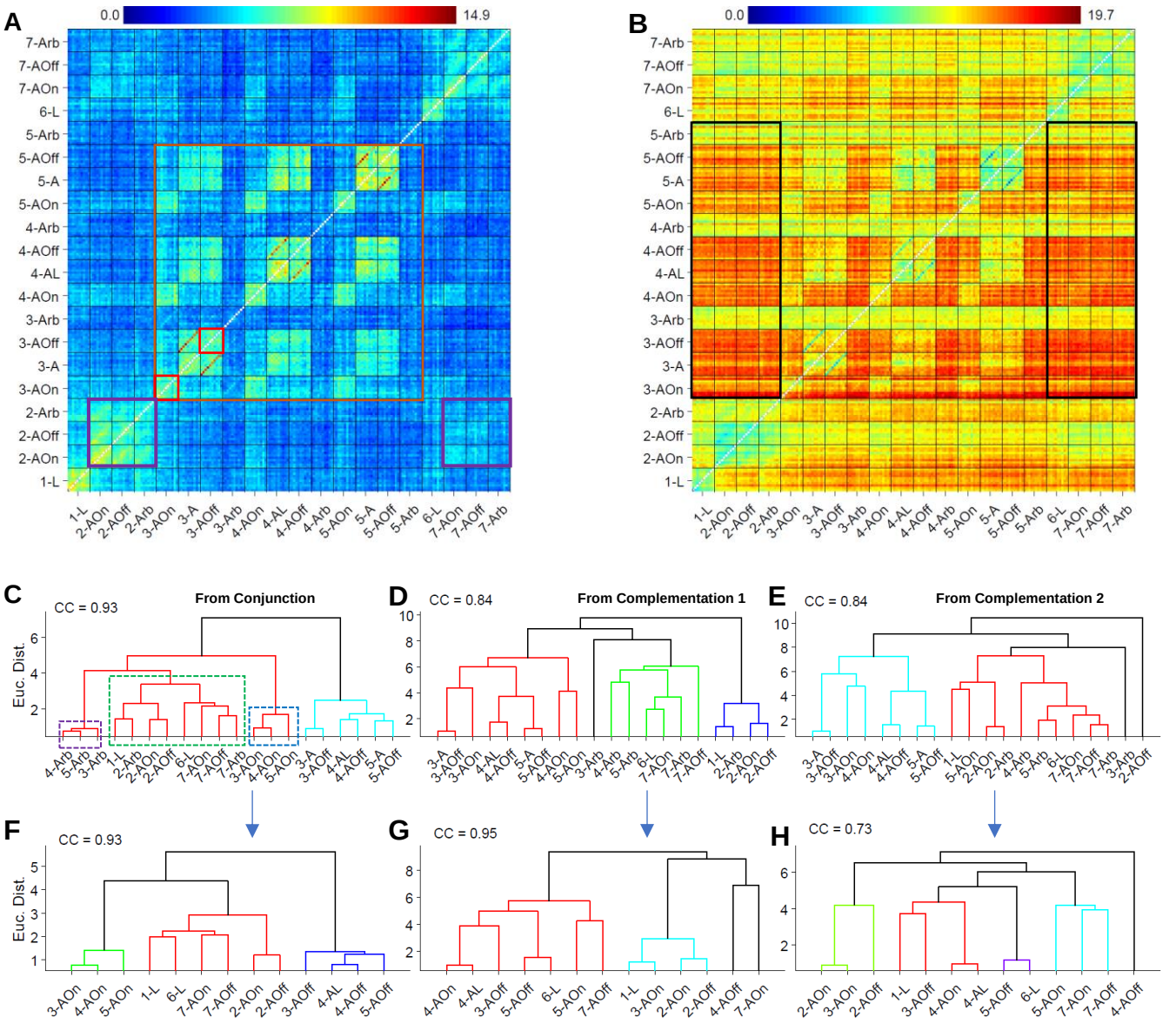

Figure 8. Trial-pair-wise dynamics of conjunction and complementation of cellular populations for all 20 sensorimotor events. **(A)** Heatmap of the average percentage of conjunctive cells between trials from all 20 events. The 200 × 200 pixels (off diagonal) belong to trial-pairs from all 20 events, as shown by the x and y labels. Each big box enclosed by thin black lines shows 10 × 10 trial pairs of the given event. For example, the color value of the pixel in row 1, column 2 indicates the percentage of conjunctive cells for trial 1 and 2 of presentation of the light stimulus. **(B)** Heatmap of the percentages of complementary cells between trial pairs (like A). Here, for example, the color value of the pixel in row 1, column 2 indicates the percentage of cells present in trial 1 and not present in trial 2. **(C-E)** Dendrograms resulting from agglomerative hierarchical clustering of the average conjunction and

complementation heatmaps/matrices. **(F-H)** Dendrograms resulting from agglomerative hierarchical clustering of the average conjunction and complementation heatmaps/matrices after excluding arbitrary events. CC indicates cophenetic correlation.

The heatmap of complementary cells (Fig. 8B) revealed a larger complementation of the NB vs. B states (outlined with purple boxes). Furthermore, the checkerboard-like pattern in the middle region of the heatmap suggests selective activation during AOn versus AOff during the NB-state. Clustering of the complementary heatmaps (Comp1 and Comp2) was done in a similar manner as described above after averaging over trial-pairs and separating the upper and lower triangular regions. Here, the clustering revealed segregation of B and NB states but with some mixing owing to the ongoing recruitment of complementary cells that were similar across events or Configurations which happened close in time. The exclusion of Arb and A events before clustering revealed similar results (Fig. 8G-H).

In summary, the results from the trial-by-trial analysis reveals similar conclusions as were derived from finding responsiveness of cells after averaging over trials. More cells were recruited during transition from B to NB-state with overall larger complementation for the NB-state. Furthermore, complementation was larger in the initial trials (novel experience) and became smaller in later trials when the experience became more familiar. Additionally, distinct smaller groups of cells encoded distinct sensorimotor events.

Discussion

Calcium imaging documented the activity of hippocampal CA1 cells and revealed different individual and collective cell population responses to sensory stimulation occurring during immobility and locomotion. Head fixed mice stood on a conveyor belt and immobility was encouraged by activating a conveyor belt brake, whereas locomotion could occur when the brake was released. Light and tactile air stimuli were systematically applied during B and NB states. Neuronal excitation or inhibition

featured a salt and pepper arrangement suggesting that responsivity was not topographically organized and did not reflect a general function such as immobility vs locomotion or arousal. Overall, ~99% of 2083 cells were active within the imaging session, with ~78% responding in relation to experimental sensory/movement events. On a given trial, combinations of sensory and locomotor events featured subpopulations of active neurons that consistently represented about ~17% of all detected neurons organized in complementary and conjunctive patterns of activation. From a large population of cells, complementary and conjunctive cells encode relatively novel and familiar experiences respectively. These results suggest that hippocampal CA1 cells participate in functional networks that distinguish sensory events in relation to ongoing moment-to-moment behavior using a recruitment with replacement strategy.

A central finding of the present study was the individuation of cell responses to events featuring configurations of light, air, locomotion, and immobility. By observing cellular responses to different sensory stimuli during multiple behavioral states in a single paradigm, this study reports an unprecedented 99% responsive cells. This responsivity could be attributed to the bias of Suite2P software in identifying only active cells. However, overall ~78% of cells (determined from average responses) were tuned to the experimentally determined stimuli and motion events, with a larger percentage of cells active during locomotion vs immobility. Previous studies have reported locomotion-related responses including sensory-spatial (Herzog et al., 2019; Komorowski et al., 2009; Manns et al., 2007; Moita et al., 2003; Zhao et al., 2020), sensory-temporal (MacDonald et al., 2013; Taxidis et al., 2020), or spatial-temporal (Haimerl et al., 2019; Kraus et al., 2013; Villette et al., 2015) populations with smaller percentages or limited numbers of active cells. For example, (Taxidis et al., 2020) studied sensory-temporal representations and reported up to 30% active cells, (Alme et al., 2014) reported the use of 11 different rooms with 30 active cells per animal (freely behaving), and (Grieves et al., 2020)

used a 3D environment and reported 756 place cells from 13 rats. That the percentage of cells responsive in all conditions in the present study was negligible argues that to fully sample hippocampal cell diversity, it is necessary to study the activity of cells during an array of sensorimotor conditions.

Although the percentage (~7%) of conjunctive cells; that is cells that were active to specific sensory-motor configurations such that C ∈ A and B, was less variable across conditions of immobility and locomotion, the percentages of complementary cells; that is cells that were active to a specific stimulus or condition such that C ∈ A not B or C ∈ B not A, were larger during locomotion. Moreover, complementary cells varied with experience (in later compared to former trials), with a larger percentage occurring in the first few trials. This observation supports the idea that ongoing cellular recruitment might depend on experience as well as moment-to-moment behavior, as novel experiences become familiar experiences. The existence of conjunctive populations across similar Configurations (e.g., 2 and 7 OR 3, 4, and 5), additionally argues that familiarity is also encoded in ongoing cell activity.

For both immobility and locomotor related cellular responses, the tactile air stimulus was more potent in eliciting sensory responses than was the visual light stimulus. There were also more cells, with higher response fidelity and stability that respond to air compared to light stimulus. This is consistent with a finding in rabbits that repetitive tactile stimulation is more potent than visual stimulation in eliciting hippocampal field potentials (Whishaw and Dyck, 1984). Here, cell responsivity could have been influenced by many factors including the shorter duration of the light stimulus (200 ms) compared to the air stimulus (5 s), differences in behavioral responses of “freezing” to the stimulus, differences in autonomic responses to the stimuli, including respiratory and pupil response changes or slight body movements by the animals. Future experiments using videography combined with calcium imaging can address these possibilities. For locomotion related cell responses, we cannot rule out higher order

responses to sensory stimulation or behavior e.g., cellular responses to an AOff event might have some contributions from a previous air or light onset event or vice versa.

This study provides insights into the sensorimotor functions of the hippocampus as a neural network. First, almost no cells were consistently active in association with all sensorimotor events, as might be expected in a system related to general arousal (Green and Arduini, 1954) or reflecting only ongoing movement (Vanderwolf, 1969). Second, cell responses were not topographically organized as is found in primary sensory and motor regions of the neocortex, supporting the idea that the hippocampus is a network system (Buzsaki, 1996). Third, cells obtain specificity with respect to sensorimotor behaviors by featuring complementary and conjunctive subpopulations. For example, a subpopulation of cells might respond in relation to a tactile air stimulus when a mouse is relatively immobile, whereas a different, complementary subpopulation might respond to the same stimulus when the mouse is moving, and a smaller, conjunctive population might respond to the stimulus in both conditions. Fourth, complementary and conjunctive subpopulation cell numbers appeared relatively fixed around average numbers of 10% and 7%, respectively.

In summary, the complementary/conjunctive specificity of CA1 cells suggests that the hippocampus is a network that encodes ongoing sensorimotor events related to movement guidance. As such cell-behavior relations are congruent with reports of the relationship between hippocampal field potentials and behavior. The complementary and conjunctive cell subpopulation organization could subserve functions that include spatial behavior (O'Keefe and Dostrovsky, 1971; O'Keefe and Nadel, 1978) and episodic learning and memory (Eichenbaum, 2004; Eichenbaum and Cohen, 2014), context representation (Bulkin et al., 2020; Rudy, 2009; Smith and Bulkin, 2014), and scene construction (McCormick et al., 2021).

Methods

Animals and surgery

Animal procedures were performed in compliance with protocols approved by the Animal Welfare Committee of the University of Lethbridge and followed the guidelines for the ethical use of animals provided by the Canadian Council on Animal Care. In total 5 mice, 3 male and 2 female Thy1-GCaMP6s [C57BL/6J-Tg(Thy1-GCaMP6s)GP4.3Dkim/J] (JAX stock #024275) hemizygous transgenic mice were used. This mouse line exhibits stable and homogenous expression of GCaMP6s over a large population of cortical and subcortical excitatory neurons (Chen et al., 2013b; Dana et al., 2014). After cranial window surgery mice were housed in individually ventilated Optimice cages (Animal Care Systems) in temperature-controlled rooms (22 °C) maintained on a 12:12 light/dark cycle (lights on during the day). Food and water were provided *ad libitum*.

Mice were implanted with chronic cranial windows at ~5-7 months of age. Mice were injected subcutaneously with buprenorphine (0.075 mg/kg) 0.5 h before surgery. Immediately prior to surgery, animals were also injected subcutaneously with 0.5 ml of a 5% dextrose, 0.9% saline solution mixed with atropine (3 µg/ml). Animals were anesthetized with isoflurane (2-3% for induction, 1-1.5% for anesthesia) and their body temperature was maintained at 37 °C using a homoeothermic monitoring system and heating pad. Lidocaine (10 mg/kg) was injected under the scalp as a local anesthetic, and a section of skin was removed with scissors to expose the skull. A craniotomy, 3 mm in diameter, was made above the right hippocampus (center at -2.0 mm AP, 1.8 mm ML, relative to bregma). The dura underlying the craniotomy was resected, and a small region of neocortex was removed by aspiration, exposing the underlying white matter. A metal cylinder (3 mm outer diameter, 1.5 mm long) with a glass coverslip attached to the bottom end using optical adhesive (NOA71, Norland) was inserted into the cavity. The coverslip was gently pushed against the tissue to reduce motion, and the cylinder was

attached to the skull using cyanoacrylate tissue adhesive (Vetbond, 3M) and dental acrylic. To allow for head-fixation of the mouse, a titanium head-plate was attached to the skull using adhesive cement (C&B Metabond, Parkell). Two rubber rings were attached to the top of the head-plate, forming a well that could be filled with distilled water for imaging with a water-immersion objective. Post-surgery, subcutaneous injections of meloxicam (7.5 mg/kg) and enrofloxacin (10 mg/kg) were administered daily for 2-3 days. Animals were allowed to recover for 3-8 weeks before behavioral training was started. The age of the animals at the time of imaging was ~8 months.

Animal training and behavioral experiment

Animals were habituated to head-fixation over 3 days. Mice were head-fixed twice per day, with sessions gradually increasing in length from 5 to 30 min. Following habituation, animals were trained to run on a linear conveyor belt 150cm in length while head fixed. The conveyor belt has been previously described (Mao et al., 2017; Mao et al., 2018). The conveyor belt was not motorized; all movement of the belt were generated by the mouse. The belt was made from Velcro material (Country Brook). Training was done in the dark, on a blank conveyor belt devoid of sensory cues. Belts were washed after every training session. Mice were trained for 20-30 min each day to run in response to a continuous, mild air stream applied to the back. A solenoid valve based automated system was used to apply a continuous mild air stream from the building's compressed air supply via a regulator. To escape this stimulus, the animal was required to run a fixed distance on the belt, after which the air puff ceased. Following an inter-trial interval of 15 s, the air stream would turn on again, initiating the next training trial. The distance the mouse was required to run was increased gradually across training trials, starting each day with 30 cm, and increasing to a maximum of 150 cm (i.e., one full turn of the belt). On a given training trial, if the mouse ran the required distance with an average speed greater than 7 cm/s, the

required distance on the next trial was incremented by 7-15 cm. If the mouse failed to achieve the target speed (e.g., due to running too slowly, delayed starting, or repeated starting and stopping), the required distance did not change between trials. Mice were trained until they could rapidly reach the maximum distance of 150 cm and achieve the target speed on >75% of trials across a training session. All mice reached criterion in 3 training sessions.

After training, mice were tested (re-trained) 10-18 days later and the following day they experienced a 7-configuration behavioral paradigm while activity of hippocampal CA1 neurons was recorded by two-photon calcium imaging. Behavioural data were simultaneously acquired and synchronized with the imaging data using a data acquisition system (Axon Digidata 1322A). These data included the distance traveled on the belt (measured by rotation encoders attached to the shafts of the treadmill wheels). A fixed reference point on the belt was also tracked, using reflective tape attached to the underside of the belt, which activated a photosensor once per belt lap. Air puff onset and offset, as well as brake and visual cue onset and offset, were controlled by a microprocessor board (Arduino Mega). The results of air training and analyses of distance and/or duration tuning from air onset and offset in Configurations 3, 4, and 5 as well as additional analyses will be presented elsewhere.

Two-photon calcium imaging

A multiphoton microscopy system (Bergamo II, Thorlabs) was used for two-photon calcium imaging. A Ti:Sapphire excitation laser (Coherent) was tuned to 920 nm, with a power of ~100 mW at the sample. Laser scanning was controlled by galvo and resonant scanners. A GaAsP photomultiplier tube was used to detect the green fluorescence signal from GCaMP6s. Samples were imaged through a 16×/0.8 NA water-immersion objective (Nikon). A black fabric cover was wrapped around the objective and head-plate to block contaminating light. For two mice, images of hippocampal CA1 pyramidal

neurons were captured from two planes, with the dorsal plane ~125 µm beneath the tissue surface and the second plane 50 µm deeper. Images were gathered at a frame rate of 29.16 Hz, but the effective frame rate for each individual plane was 9.72 Hz (29.16 ÷ 3, because 1 extra fly-back frame was also captured). For three mice images were gathered from only one plane with a frame rate of 29.16Hz. A field of view of 418 × 418 µm was captured with a resolution of 512 × 512 pixels.

Data analysis

Suite2P (Pachitariu et al., 2017) (http://mouseland.github.io/suite2p) was used to register images and to automatically detect regions of interest (ROIs) assumed to represent individual cell bodies. Raw calcium traces were determined for each ROI by averaging the fluorescence signal from all pixels within the ROI and correcting for neuropil contamination. For each raw calcium fluorescence trace (F), baseline (F_o) was estimated, and baseline subtracted signal ($\Delta F/F_o$) was then determined as $(F-F_o)/F_o$. From the $\Delta F/F_o$ calcium traces, deconvolved spike rates were determined using a first order auto-regressive model and constrained nonnegative matrix factorization (Friedrich et al., 2017). Further analysis of the deconvolved traces was conducted using custom scripts written in MATLAB (MathWorks).

Agglomerative Hierarchical Clustering

This analysis was performed on the conjunction or complementation matrices (heatmaps) when multiple cell groups were considered. Complementation matrices were split into two heatmaps symmetric across the diagonal by using the upper and lower triangular matrices corresponding to Comp1 and Comp2 types of cells before clustering. Based on the conjunction and complementation percentages of each cell group with every other cell group, this analysis found cell groups which were like each other

i.e., close to each other with respect to their relationships with all other cell groups. The analysis was done by first calculating Euclidian distance for each pair of cell groups considering two rows of a matrix at a time (using Matlab function "pdist"). For example, if a matrix was n x n, there would be $\frac{n!}{2!(n-2)!}$ pairs which can then be arranged into a symmetric n x n matrix usually called the dissimilarity matrix owing to smaller Euclidian distance indicating smaller dissimilarity. Matlab function "linkage" was then used to operate on the dissimilarity matrix and define clusters based on the unweighted average distance between clusters. Clusters were then separated (color coded in figures using the Matlab function "dendrogram") by using a threshold of 70% of the maximum linkage distance between any two clusters. The quality of clustering was assessed by determining cophenetic correlation (CC) reported with each dendrogram in figures.

Statistical Analysis

Statistical analysis was done in Matlab® 2018b (Ver 9.5.0.944444) and confirmed for accuracy with IBM® SPSS® (Ver 28.0.1.1). All means in the text are reported ± the standard error of the mean (SEM). Unless otherwise specified, a repeated measures analysis of variance (RM-ANOVA) test was used for statistically comparing differences in measured parameters from n = 5 animals. Shapiro-Wilk test was used for test of normality and was done using a file "swtest.m" downloaded from Matlab File Exchange Server (BenSaïda, 2022). The accuracy of the code was confirmed by comparing its output with similar results from SPSS. Minor violations of the normality test and the presence of outliers were ignored e.g., if some variables did not pass the normality test or had outliers, RM-ANOVA was still performed. The test for sphericity was conducted using Mauchly's Test. Greenhouse-Geisser corrected *p*-value is reported where sphericity was violated. All post hoc pairwise comparisons were conducted

either using Tukey's Honestly Significant Difference (HSD) test or Bonferroni correction with an alpha = 0.05.

An alpha value of .05 was used to determine significance at the first level of analysis e.g., for performing a three-way RM-ANOVA. For the second level of analysis, it was adjusted with Bonferroni correction e.g., if there was a significant three-way interaction, in the second level of analysis to find simple two-way interactions, alpha was divided by the number of statistical tests performed. For example, if there were two simple two-way interactions to be tested, an alpha value of 0.05/2 = 0.025 was used. Similarly, at the next level of analysis, alpha was further divided by the number of statistical comparisons made e.g., if there were three simple simple main effects to be tested, alpha = 0.025/3 = 0.0083 was used. *, **, and *** indicate *p*-values less than .05, .01, and .001, respectively. Actual *p*-values are reported except for values less than .001 are reported as $p < .001$. Because of the small sample size (n = 5 animals), effect size is reported along with *p*-values as partial η^2 = (Sum of Squares $_{effect}$)/(Sum of Squares $_{effect}$ + Sum of Squares $_{error}$).

Acknowledgements

We thank Dr. JianJun Sun for performing animal surgeries, Di Shao and the University of Lethbridge Animal Care Services staff for animal husbandry, and HaoRan Chang, Dr. Hardeep Ryait, and Žaneta Navrátilová for useful discussions regarding the preparation of this manuscript.

Author Contributions

All authors participated in the design of this study, with SI and IQW as the main contributors. SI and BBM performed the experiments. SI performed the data analyses with participation of the other

authors. SI and IQW wrote the manuscript, which all authors commented on and edited. BLM and MHM supervised the study.

References

Alme, C.B., Miao, C., Jezek, K., Treves, A., Moser, E.I., and Moser, M.B. (2014). Place cells in the hippocampus: eleven maps for eleven rooms. Proceedings of the National Academy of Sciences of the United States of America *111*, 18428-18435.
Arriaga, M., and Han, E.B. (2017). Dedicated Hippocampal Inhibitory Networks for Locomotion and Immobility. The Journal of neuroscience : the official journal of the Society for Neuroscience *37*, 9222-9238.
Attinger, A., Wang, B., and Keller, G.B. (2017). Visuomotor Coupling Shapes the Functional Development of Mouse Visual Cortex. Cell *169*, 1291-1302 e1214.
Ayaz, A., Stauble, A., Hamada, M., Wulf, M.A., Saleem, A.B., and Helmchen, F. (2019). Layer-specific integration of locomotion and sensory information in mouse barrel cortex. Nature communications *10*, 2585.
Bellistri, E., Aguilar, J., Brotons-Mas, J.R., Foffani, G., and de la Prida, L.M. (2013). Basic properties of somatosensory-evoked responses in the dorsal hippocampus of the rat. The Journal of physiology *591*, 2667-2686.
BenSaïda, A. (2022). Shapiro-Wilk and Shapiro-Francia normality tests. In MATLAB Central File Exchange (MATLAB Central File Exchange: MathWorks).
Bulkin, D.A., Sinclair, D.G., Law, L.M., and Smith, D.M. (2020). Hippocampal state transitions at the boundaries between trial epochs. Hippocampus *30*, 582-595.
Buzsaki, G. (1996). The hippocampo-neocortical dialogue. Cerebral cortex (New York, NY : 1991) *6*, 81-92.
Buzsáki, G. (2006). Rhythms of the brain (New York, NY, US: Oxford University Press).
Buzsaki, G., and Watson, B.O. (2012). Brain rhythms and neural syntax: implications for efficient coding of cognitive content and neuropsychiatric disease. Dialogues Clin Neurosci *14*, 345-367.
Chen, G., King, J.A., Burgess, N., and O'Keefe, J. (2013a). How vision and movement combine in the hippocampal place code. Proceedings of the National Academy of Sciences of the United States of America *110*, 378-383.
Chen, T.W., Wardill, T.J., Sun, Y., Pulver, S.R., Renninger, S.L., Baohan, A., Schreiter, E.R., Kerr, R.A., Orger, M.B., Jayaraman, V., *et al.* (2013b). Ultrasensitive fluorescent proteins for imaging neuronal activity. Nature *499*, 295-300.
Clancy, K.B., Orsolic, I., and Mrsic-Flogel, T.D. (2019). Locomotion-dependent remapping of distributed cortical networks. Nature neuroscience *22*, 778-786.
Colgin, L.L. (2020). Five Decades of Hippocampal Place Cells and EEG Rhythms in Behaving Rats. The Journal of neuroscience : the official journal of the Society for Neuroscience *40*, 54-60.
Dana, H., Chen, T.W., Hu, A., Shields, B.C., Guo, C., Looger, L.L., Kim, D.S., and Svoboda, K. (2014). Thy1-GCaMP6 transgenic mice for neuronal population imaging in vivo. PloS one *9*, e108697.
Dipoppa, M., Ranson, A., Krumin, M., Pachitariu, M., Carandini, M., and Harris, K.D. (2018). Vision and Locomotion Shape the Interactions between Neuron Types in Mouse Visual Cortex. Neuron *98*, 602-615 e608.
Eichenbaum, H. (2004). Hippocampus: cognitive processes and neural representations that underlie declarative memory. Neuron *44*, 109-120.
Eichenbaum, H., Amaral, D.G., Buffalo, E.A., Buzsaki, G., Cohen, N., Davachi, L., Frank, L., Heckers, S., Morris, R.G., Moser, E.I., *et al.* (2016). Hippocampus at 25. Hippocampus *26*, 1238-1249.
Eichenbaum, H., and Cohen, N.J. (2014). Can we reconcile the declarative memory and spatial navigation views on hippocampal function? Neuron *83*, 764-770.
Foster, T.C., Castro, C.A., and McNaughton, B.L. (1989). Spatial selectivity of rat hippocampal neurons: dependence on preparedness for movement. Science *244*, 1580-1582.
Friedrich, J., Zhou, P., and Paninski, L. (2017). Fast online deconvolution of calcium imaging data. In PLoS computational biology.

Green, J.D., and Arduini, A.A. (1954). Hippocampal electrical activity in arousal. Journal of neurophysiology *17*, 533-557.
Grieves, R.M., Jedidi-Ayoub, S., Mishchanchuk, K., Liu, A., Renaudineau, S., and Jeffery, K.J. (2020). The place-cell representation of volumetric space in rats. Nature communications *11*, 789.
Haimerl, C., Angulo-Garcia, D., Villette, V., Reichinnek, S., Torcini, A., Cossart, R., and Malvache, A. (2019). Internal representation of hippocampal neuronal population spans a time-distance continuum. Proceedings of the National Academy of Sciences of the United States of America *116*, 7477-7482.
Herzog, L.E., Pascual, L.M., Scott, S.J., Mathieson, E.R., Katz, D.B., and Jadhav, S.P. (2019). Interaction of Taste and Place Coding in the Hippocampus. The Journal of neuroscience : the official journal of the Society for Neuroscience *39*, 3057-3069.
Igarashi, K.M., Lu, L., Colgin, L.L., Moser, M.B., and Moser, E.I. (2014). Coordination of entorhinal-hippocampal ensemble activity during associative learning. Nature *510*, 143-147.
Itskov, P.M., Vinnik, E., and Diamond, M.E. (2011). Hippocampal representation of touch-guided behavior in rats: persistent and independent traces of stimulus and reward location. PloS one *6*, e16462.
Kay, K., and Frank, L.M. (2019). Three brain states in the hippocampus and cortex. Hippocampus *29*, 184-238.
Kay, K., Sosa, M., Chung, J.E., Karlsson, M.P., Larkin, M.C., and Frank, L.M. (2016). A hippocampal network for spatial coding during immobility and sleep. Nature *531*, 185-190.
Keller, G.B., Bonhoeffer, T., and Hubener, M. (2012). Sensorimotor mismatch signals in primary visual cortex of the behaving mouse. Neuron *74*, 809-815.
Komorowski, R.W., Manns, J.R., and Eichenbaum, H. (2009). Robust conjunctive item-place coding by hippocampal neurons parallels learning what happens where. The Journal of neuroscience : the official journal of the Society for Neuroscience *29*, 9918-9929.
Kramis, R., Vanderwolf, C.H., and Bland, B.H. (1975). Two types of hippocampal rhythmical slow activity in both the rabbit and the rat: relations to behavior and effects of atropine, diethyl ether, urethane, and pentobarbital. Exp Neurol *49*, 58-85.
Kraus, B.J., Robinson, R.J., 2nd, White, J.A., Eichenbaum, H., and Hasselmo, M.E. (2013). Hippocampal "time cells": time versus path integration. Neuron *78*, 1090-1101.
MacDonald, C.J., Carrow, S., Place, R., and Eichenbaum, H. (2013). Distinct hippocampal time cell sequences represent odor memories in immobilized rats. The Journal of neuroscience : the official journal of the Society for Neuroscience *33*, 14607-14616.
Manns, J.R., Howard, M.W., and Eichenbaum, H. (2007). Gradual changes in hippocampal activity support remembering the order of events. Neuron *56*, 530-540.
Mao, D., Kandler, S., McNaughton, B.L., and Bonin, V. (2017). Sparse orthogonal population representation of spatial context in the retrosplenial cortex. In Nature communications.
Mao, D., Neumann, A.R., Sun, J., Bonin, V., Mohajerani, M.H., and McNaughton, B.L. (2018). Hippocampus-dependent emergence of spatial sequence coding in retrosplenial cortex. Proceedings of the National Academy of Sciences of the United States of America *115*, 8015-8018.
McCormick, C., Dalton, M.A., Zeidman, P., and Maguire, E.A. (2021). Characterising the hippocampal response to perception, construction and complexity. Cortex *137*, 1-17.
Mineault, P.J., Tring, E., Trachtenberg, J.T., and Ringach, D.L. (2016). Enhanced Spatial Resolution During Locomotion and Heightened Attention in Mouse Primary Visual Cortex. The Journal of neuroscience : the official journal of the Society for Neuroscience *36*, 6382-6392.
Moita, M.A., Rosis, S., Zhou, Y., LeDoux, J.E., and Blair, H.T. (2003). Hippocampal place cells acquire location-specific responses to the conditioned stimulus during auditory fear conditioning. Neuron *37*, 485-497.
Moser, E.I., Moser, M.B., and McNaughton, B.L. (2017). Spatial representation in the hippocampal formation: a history. Nature neuroscience *20*, 1448-1464.
Musall, S., Kaufman, M.T., Juavinett, A.L., Gluf, S., and Churchland, A.K. (2019). Single-trial neural dynamics are dominated by richly varied movements. Nature neuroscience *22*, 1677-1686.
Niell, C.M., and Stryker, M.P. (2010). Modulation of visual responses by behavioral state in mouse visual cortex. Neuron *65*, 472-479.

O'Keefe, J., and Dostrovsky, J. (1971). The hippocampus as a spatial map. Preliminary evidence from unit activity in the freely-moving rat. Brain research *34*, 171-175.
O'Keefe, J., and Nadel, L. (1978). The Hippocampus as a Cognitive Map (Oxford: Clarendon Press).
Pachitariu, M., Stringer, C., Dipoppa, M., Schröder, S., Rossi, L.F., Dalgleish, H., Carandini, M., and Harris, K.D. (2017). Suite2p: beyond 10,000 neurons with standard two-photon microscopy. bioRxiv.
Perentos, N., Krstulovic, M., and Morton, A.J. (2022). Deep brain electrophysiology in freely moving sheep. Current biology : CB *32*, 763-774 e764.
Rudy, J.W. (2009). Context representations, context functions, and the parahippocampal-hippocampal system. Learning & memory (Cold Spring Harbor, NY) *16*, 573-585.
Sakurai, Y. (2002). Coding of auditory temporal and pitch information by hippocampal individual cells and cell assemblies in the rat. Neuroscience *115*, 1153-1163.
Saleem, A.B., Diamanti, E.M., Fournier, J., Harris, K.D., and Carandini, M. (2018). Coherent encoding of subjective spatial position in visual cortex and hippocampus. Nature *562*, 124-127.
Schneider, D.M. (2020). Reflections of action in sensory cortex. Current opinion in neurobiology *64*, 53-59.
Schneider, D.M., Nelson, A., and Mooney, R. (2014). A synaptic and circuit basis for corollary discharge in the auditory cortex. Nature *513*, 189-194.
Smith, D.M., and Bulkin, D.A. (2014). The form and function of hippocampal context representations. Neuroscience and biobehavioral reviews *40*, 52-61.
Sofroniew, N.J., Vlasov, Y.A., Hires, S.A., Freeman, J., and Svoboda, K. (2015). Neural coding in barrel cortex during whisker-guided locomotion. Elife *4*.
Souza, B.C., Pavao, R., Belchior, H., and Tort, A.B.L. (2018). On Information Metrics for Spatial Coding. Neuroscience *375*, 62-73.
Stringer, C., Pachitariu, M., Steinmetz, N., Reddy, C.B., Carandini, M., and Harris, K.D. (2019). Spontaneous Behaviors Drive Multidimensional, Brain-wide Activity. Science *364*, 255.
Taxidis, J., Pnevmatikakis, E.A., Dorian, C.C., Mylavarapu, A.L., Arora, J.S., Samadian, K.D., Hoffberg, E.A., and Golshani, P. (2020). Differential Emergence and Stability of Sensory and Temporal Representations in Context-Specific Hippocampal Sequences. Neuron *108*, 984-998 e989.
Vanderwolf, C.H. (1969). Hippocampal electrical activity and voluntary movement in the rat. Electroencephalogr Clin Neurophysiol *26*, 407-418.
Vanderwolf, C.H., Gutman, M., and Baker, G.B. (1984). Hypothalamic self-stimulation: the role of dopamine and possible relations to neocortical slow wave activity. Behavioural brain research *12*, 9-19.
Villette, V., Malvache, A., Tressard, T., Dupuy, N., and Cossart, R. (2015). Internally Recurring Hippocampal Sequences as a Population Template of Spatiotemporal Information. Neuron *88*, 357-366.
Wang, Y., Feng, Z., Wang, J., and Zheng, X. (2014). Somatosensory stimulation suppresses the excitability of pyramidal cells in the hippocampal CA1 region in rats. Neural Regen Res *9*, 1138-1144.
Whishaw, I.Q. (1976). The effects of alcohol and atropine on EEG and behavior in the rabbit. Psychopharmacology (Berl) *48*, 83-90.
Whishaw, I.Q., and Dyck, R. (1984). Comparative potency of tactile, auditory, and visual stimulus repetition in eliciting activated forebrain EEG in the rabbit. Behavioral neuroscience *98*, 333-344.
Whishaw, I.Q., and Vanderwolf, C.H. (1971). Hippocampal EEG and behavior: effects of variation in body temperature and relation of EEG to vibrissae movement, swimming and shivering. Physiol Behav *6*, 391-397.
Whishaw, I.Q., and Vanderwolf, C.H. (1973). Hippocampal EEG and behavior: changes in amplitude and frequency of RSA (theta rhythm) associated with spontaneous and learned movement patterns in rats and cats. Behav Biol *8*, 461-484.
Yu, J.Y., Kay, K., Liu, D.F., Grossrubatscher, I., Loback, A., Sosa, M., Chung, J.E., Karlsson, M.P., Larkin, M.C., and Frank, L.M. (2017). Distinct hippocampal-cortical memory representations for experiences associated with movement versus immobility. Elife *6*.
Zhao, X., Wang, Y., Spruston, N., and Magee, J.C. (2020). Membrane potential dynamics underlying context-dependent sensory responses in the hippocampus. Nature neuroscience *23*, 881-891.